IEEE Access
Multidisciplinary ⋮ Rapid Review ⋮ Open Access Journal

Received 10 March 2023, accepted 26 March 2023, date of publication 31 March 2023, date of current version 5 April 2023.

Digital Object Identifier 10.1109/ACCESS.2023.3263528

RESEARCH ARTICLE

Robust Adaptive Backstepping Control of Quadrotors With Unknown Input Gains

JENG-TZE HUANG, (Senior Member, IEEE), AND YU-WEI JIANG
Institute of Digital Mechatronic Technology, Chinese Culture University, Taipei 11114, Taiwan

Corresponding author: Jeng-Tze Huang (hzz4@ulive.pccu.edu.tw)

This work was supported in part by the National Science and Technology Council, Taiwan, under Grant MOST 111-2221-E-034-005.

ABSTRACT Robust adaptive tracking control design for quadrotors with unknown parameters, including the thrust and the drag factors, is presented. Firstly, the adaptive linearizing control approach is employed for conquering the issues of unknown input gains in both the outer- and inner-loop design steps. Secondly, based on the barrier Lyapunov function (BLF) method, a robust virtual controller is constructed in the intermediate design step for counteracting the coupling nonlinearity and speeding up the convergence at the same time. Thirdly, the dynamic surface control (DSC) technique is applied for alleviating the measurement of acceleration signals and explosion of complexity problem simultaneously. Last, the serial-parallel identification model (SPIM) based composite update algorithms are incorporated for further improving the tracking performance. In particular, the prediction errors are ensured to converge to the vicinity of zero without relying on the parameter convergence. Simulation studies demonstrating its validity are carried out in the final.

INDEX TERMS Composite update algorithm, quadrotors, robust adaptive, unknown input gains.

I. INTRODUCTION

Motivated by its wide variety of applications, control of quadrotors has attracted lots of attentions in both the academic and industrial fields in recent years ([1], [2], [3], [4], [5], [6], [7], [8], [9], and the references in [10]). It is quite a challenging task for the under-actuated and highly nonlinear coupling features of the system [2], [11]. In this regard, the backstepping tool is widely adopted for tackling such a task and a vast of relevant control algorithms are now available in the literature [12], [13], [14], [15], [16], [17]. Among others, the adaptive backstepping control is applied for dealing with the parametric uncertainty in mass, inertia, viscosity, etc, while the robust backstepping control is for coping with nonparametric uncertainty, e.g., the wind turbulence, nonlinear coupling, etc. [10], [12], [18]. Noticeably, most of the aforementioned works use the thrust force and torques as their control inputs, of which the required motors' rotary speeds can be directly calculated when the proportional constants, namely, the thrust and the drag factors, are available (see [10], [11] and references therein). Unfortunately, these two constants are difficult to attain in real operations since they vary with some environmental factors such as the air density, lift constant, etc. [2], [6], [19].

Clearly, it is more practical to use the motors' speeds as the control inputs instead. The task turns into the control design with uncertain input gains based on a state-space model. First, via estimating the reciprocal of the input gains, the immersion and invariance (I&I) based saturated guidance control law in [20] conquered the limited thrust force without igniting the control singularity at the same time. The I&I method was also adopted in the outer-loop design of [21] for estimating the unknown viscosity-to-mass ratio. To detour the difficulty, another common approach is to launch the control synthesis based on the physical model with unity input gains. However, such a model is not affable to the incorporation of standard identification schemes for performance improvement [12].

The standard backstepping design starts from stabilizing the translational (outer-loop) tracking error dynamics via using the nonlinear coupling term as the virtual control input. Next, the inner-loop control is activated to manage the error between the coupling nonlinearity and the virtual controller

The associate editor coordinating the review of this manuscript and approving it for publication was Yang Tang.

to converge to zero [16]. Under such an architecture, the hierarchical control uses the time-scale separation (TSS) feature between the translational (slow) dynamics and the rotational (fast) dynamics to separately design the controllers and then invokes the singular perturbation method for stability analysis [16], [17], [22]. The passivity-based approach considered the translational and the rotational dynamics as two interconnected passive subsystems. The control task reduces to the asymptotic stabilization of two uncoupled tracking error subsystems [21], [23]. Noticeably, the former approach calls for high control gains while the latter may involve discontinuous control for ensuring the asymptotic stability in the presence of exogenous disturbances [21]. On the other hand, the saturation control is an alternative without resorting to the TSS and asymptotic stability [24]. However, the corresponding domain of attraction is hard to prescribe beforehand.

Adaptive control is known to suffer from poor transient behaviors in general [12], [18], [25]. Via including the prediction-error terms into the update algorithm, the so-called composite adaptive control is a popular approach for alleviating such a drawback in the literature [24], [26]. To name a few, the direct and indirect model reference adaptive control in [27] includes a bilinear predictor model to generate the prediction error and improving the tracking performance of quadrotors. The article in [24] proposed a saturated adaptive I&I-based control strategy for the trajectory tracking of quadrotor systems. Shao et al. proposed an I&I-based adaptive controller for anti-unwinding attitude maneuvers [28]. Noticeably, performance improvement in these works relies on parameter convergence, which in turn imposes certain excitation criteria on the regressors, such as persistent excitation [18], [29], internal excitation [30], cooperative finite-time excitation [31], etc. In contrast, the composite adaptive control in [32] guaranteed the convergence of prediction errors to a small set around zero without any excitation criteria. However, it cannot be directly applied to the quadrotors which are not in the linearizable canonical form.

In this regard, we aim to synthesize a robust adaptive tracking controller for tackling the aforementioned issues in this article. First, considering its ease of incorporating the standard serial-parallel identification model (SPIM) [29], the adaptive linearizing control is adopted in the inner- and outer-loop design [32]. The possible control singularity is prevented via the parameter projection method [12]. Next, a barrier Lyapunov function (BLF)-based robust virtual controller is built in the intermediate design step for suppressing the coupling nonlinearity and speeding up the convergence at the same time. The dynamic surface control (DSC) technique is applied for alleviating the measurement of acceleration signals and the explosion of complexity problem simultaneously [33] and [34]. Last, an SPIM-based composite update algorithm guaranteeing the convergence of prediction errors, is incorporated to further improve the tracking performance. The main contributions of the paper are summarized as follows.

i) The rotors' speeds instead of the popular thrust force and torques are utilized as the control inputs.
ii) The residual coupling nonlinearity is directly compensated without resorting to the TSS or passivity features of the system.
iii) The adopted SPIM-based composite update law ensures the convergence of prediction errors without relying on the parameter convergence, which in turn improves the tracking performance.

The rest of the article is arranged as follows. Section II describes the system model and the tackled problems. Section III presents the controller design and the corresponding stability analysis. Section IV carries out some numerical studies to demonstrate the validity of the proposed design. Conclusion is finally drawn in Section V.

A. PRELIMINARY

In this paper, $|\xi|$ denotes the absolute value or Euclidean norm when ξ is a scalar or a vector, respectively; $\hat{(\cdot)}$ is the estimation of an unknown parameter vector $(\cdot)$ and $\tilde{(\cdot)} = (\cdot)-\hat{(\cdot)}$. The componentwise multiplication of any two vectors $x, y \in R^3$ is defined as $x.*y = col[x_1y_1, x_2y_2, x_3y_3]$. $\tanh(x) = col[\tanh(x_1), \tanh(x_2), \tanh(x_3)]$, $x^\wedge = [0, -x_3, x_2; x_3, 0, -x_1; -x_2, x_1, 0]^T$ and $(x^\wedge)^\vee = x$.

Lemma 1 ([3]): For $y \in R^3$ and $M \in R^{3\times3}$, the following equality holds:

$$tr(My^\wedge) = -y^T(M - M^T)^\vee \tag{1}$$

Lemma 2 ([1] and [16]): For $y \in R^3$, $R \in SO(3)$ with rotation axis $\hat{k}$ and angle ξ, the following equalities hold:

$$|\frac{(R - R^T)^\vee}{2}| = \cos\frac{\xi}{2}\sqrt{tr(I - R)} \tag{2}$$

$$tr(I - R) = 2(1 - \cos\xi) \tag{3}$$

$$R(y)^\wedge R^T = (Ry)^\wedge \tag{4}$$

Lemma 3 ([17]): For $x \in \Re$, if $x \in [0, k)$, the following inequality holds:

$$\ln\frac{k}{k - x} \le \frac{x}{k - x} \tag{5}$$

The standard projection algorithm is in a form of

$$\dot{\hat{\theta}} = \mathcal{P}(\sigma), \tag{6}$$

where $\hat{\theta}$ is the estimation of the unknown parameter vector θ, which lies within a prescribed compact convex set $\Omega_\theta \subset R^p$, and σ is the function such that $\dot{\hat{\theta}} = \sigma$, whenever $\hat{\theta}$ stays in the interior of Ω_θ. It ensures that [12]
P1): $\hat{\theta}(t) \in \Omega_\theta, \forall t \ge 0$, whenever $\hat{\theta}(0) \in \Omega_\theta$;
P2): $-\tilde{\theta}^T Proj(\sigma) \le -\tilde{\theta}^T\sigma$.

The following inequality is essential to the subsequent stability analysis [35]

$$0 \le |\varsigma| - \varsigma\tanh(\frac{\varsigma}{w_0}) \le c_\varsigma w_0, \quad \forall\varsigma \in R, \tag{7}$$

where $c_\varsigma = 0.2785$ and w_0 is a positive constant.

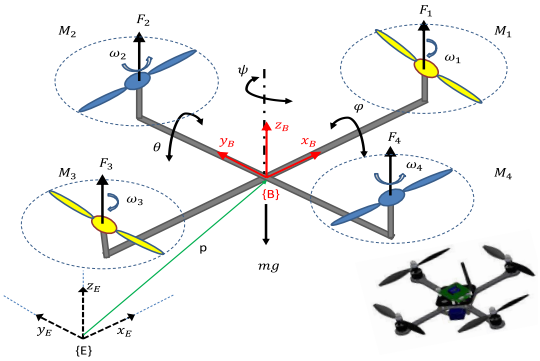

FIGURE 1. Configuration of a quadrotor.

II. SYSTEM MODEL

The quadrotor's configuration depicted in Fig. 1 is generally described in two reference frames, a stationary inertial frame $E = \{x_E, y_E, z_E\}$ and a body frame $B = \{x_B, y_B, z_B\}$ located at O_E and the center of mass O_B, respectively. Let $p = [p_x, p_y, p_z]^T$ and $v = [v_x, v_y, v_z]^T$ denote the position and the translational velocity of O_B in frame E, respectively, and $\Omega = [\Omega_x, \Omega_y, \Omega_z]^T$ denotes the angular velocity of the vehicle in frame B. The physical model of a quadrotor is given by

$$\dot{p} = v \tag{8a}$$

$$\dot{v} = -g\hat{z} + \frac{T}{m}R\hat{z} \tag{8b}$$

$$\dot{R} = R\Omega^{\wedge} \tag{8c}$$

$$J\dot{\Omega} = -\Omega^{\wedge}J\Omega + \tau \tag{8d}$$

$$J_m\dot{\omega}_i = \tau_{m,i} - Q_i, \tag{8e}$$

where $i = 1, \cdots, 4$, m is the mass, $J = diag\{J_x, J_y, J_z\}$ is the inertial matrix, $\hat{z} = [0, 0, 1]^T$ is the third basis vector of R^3, $g = 9.81\ m/s^2$, $T \in R$ and $\tau = [\tau_x, \tau_y, \tau_z]^T$ denote the applied thrust force and torque generated by the four rotors in frame $\mathcal{B}$, respectively, J_m is the inertia of the motor, ω_i and $\tau_{m,i}$, are the rotary speed and torque of the i,th motor, respectively, Q_i is the reactive torque (due to rotor drag), and $R \in SO(3)$ is the rotation matrix which, in terms of the Euler angle $\varpi = (\phi, \theta, \psi)^T$, is given by [15]

$$R = \begin{bmatrix} c_\theta c_\psi & s_\phi s_\theta c_\psi - c_\phi s_\psi & c_\phi s_\theta c_\psi + s_\phi s_\psi \\ c_\theta s_\psi & s_\phi s_\theta s_\psi + c_\phi c_\psi & c_\phi s_\theta s_\psi - s_\phi c_\psi \\ -s_\theta & s_\phi c_\theta & c_\phi c_\theta \end{bmatrix} \tag{9}$$

where c_* and s_* are the abbreviations for $\cos(*)$ and $\sin(*)$, respectively.

Based on (8c) and (9), $\dot{\varpi}$ is related to Ω by

$$\dot{\varpi} = W\Omega \tag{10}$$

where

$$W = \frac{1}{c_\theta}\begin{bmatrix} c_\theta & s_\theta s_\phi & s_\theta c_\phi \\ 0 & c_\theta c_\phi & -c_\theta s_\phi \\ 0 & s_\phi & c_\phi \end{bmatrix} \tag{11}$$

Clearly, W is invertible for all $\theta \neq (2k-1)\pi/2$.

The reactive torque may be modeled as [15]

$$Q_i = \kappa\omega_i^2, \tag{12}$$

where κ is the drag factor. It then enters (8d) as a part of the total torque τ, which may contain additional components, such as disturbances, gyroscopic torques, etc. By ignoring these minor contributions for simplicity, the thrust force T and the torque vector τ can be expressed in terms of the motors' speeds ω_i, $i = 1, 2, 3, 4$ as [2], [3], [4], [5], [6], [7], [8], [9], [10], [11], [12], [13], [14], and [15]

$$\begin{bmatrix} T \\ \tau_x \\ \tau_y \\ \tau_z \end{bmatrix} = \begin{bmatrix} b & b & b & b \\ 0 & -bl & 0 & bl \\ bl & 0 & -bl & 0 \\ \kappa & -\kappa & \kappa & -\kappa \end{bmatrix}\begin{bmatrix} \omega_1^2 \\ \omega_2^2 \\ \omega_3^2 \\ \omega_4^2 \end{bmatrix} \tag{13}$$

where l is the distance from O_B to the rotation axis of each rotor, while b denotes the thrust factor.

The following two assumptions are essential to the subsequent control design.

- *Assumption 1:* The reference dignals $d^i p_c(t)/dt^i$ and $d^i\psi_c(t)/dt^i$, $i = 0, 1, 2$ are bounded and known *a priori*.
- *Assumption 2:* The signals $d^i p(t)/dt^i$ and $d^i\varpi(t)/dt^i$, $i = 0, 1$ are measurable.
- *Assumption 3:* The Euler angles are bounded by $-\frac{\pi}{2} < \phi < \frac{\pi}{2}, -\frac{\pi}{2} < \theta < \frac{\pi}{2}, -\pi < \psi < \pi$.

The control input $u = col[u_1, u_2, u_3, u_4] \in R^4$ in this article is defined by

$$u = A\omega .* \omega = \begin{bmatrix} 1 & 1 & 1 & 1 \\ 0 & -1 & 0 & 1 \\ 1 & 0 & -1 & 0 \\ 1 & -1 & 1 & -1 \end{bmatrix}\begin{bmatrix} \omega_1^2 \\ \omega_2^2 \\ \omega_3^2 \\ \omega_4^2 \end{bmatrix} \tag{14}$$

Although such control inputs have also been utilized in some works [15], [36], [37], however, so far they are restricted for cases with known input gains. Accordingly, (13) can be rewritten as

$$\begin{bmatrix} T \\ \tau_x \\ \tau_y \\ \tau_z \end{bmatrix} = \begin{bmatrix} bu_1 \\ blu_2 \\ blu_3 \\ \kappa u_4 \end{bmatrix} \tag{15}$$

- *Assumption 4:* The motor's dynamics in (8e) is negligible compared to the vehicle dynamics in (8a)-(8d).

Remark 1: The system model (8a)-(8e) consists of the vehicle dynamics (8a)-(8d) and the motor dynamics (8e), with the latter coupled to the former via the rotors' speeds. By virtue of Assumption 4, we only need to focus on the vehicle dynamics via using either the popular (T, τ) pair or u in (14) as the control inputs. In either cases, the synthesized control law should next be transformed to the commands for the motor subsystem to track in practice [15], [36], [37]. It should be noted that such a procedure cannot be carried out in the former case when the input gains are uncertain. Consequently, the proposed design is more suitable under such circumstances.

Control objective: This article aims to synthesize a control strategy for the tracking of a reference command $(p_c(t), \psi_c(t))$ in the presence of parametric uncertainty in m, J, l, b, and κ.

To that end, three major challenges have to be conquered a) manipulation of the residual coupling nonlinearity without resorting to the TSS or passivity properties; b) avoidance of the measurement of acceleration signals and the explosion of complexity problem while preserving stability of the closed-loop system at the same time; c) development of a composite update algorithm for ensuring the convergence of the prediction errors and hence improving the tracking performance.

III. CONTROL SYNTHESIS

The control design consists of two consecutive steps, i.e., the outer-loop and the inner-loop designs. In particular, the residual nonlinear coupling term appearing in the former is suppressed via a robust control component in the latter, followed by the DSC technique for preventing the consequent measurement of acceleration signals and the explosion of complexity problem, etc. Last, SPIM-based composite update algorithms, which ensure the convergence of the prediction errors to the vicinity of zero, are incorporated. Details are given in the following.

A. OUTER-LOOP DESIGN

Define the auxiliary tracking error vector

$$z_p = v_e + \lambda_a p_e + \lambda_b \int_0^t p_e(\eta) d\eta, \tag{16}$$

where $\lambda_a, \lambda_b > 0$ are gain constants, $p_e = p - p_c$, and $v_e = v - \dot{p}_c$.

By a direct differentiation of z_p, it yields

$$\dot{z}_p = -(g\hat{z} + \ddot{p}_c) + \lambda_a v_e + \lambda_b p_e + \theta_t u_1 R\hat{z} \tag{17}$$

where $\theta_t = b/m$.

To stabilize the z_p dynamics in (17), the rotation matrix R should provide appropriate coupling forces. Denote such a matrix by R_c and treat $\alpha = u_1 R_c \hat{z}$ as the control input. Equation (17) can be rewritten as

$$\dot{z}_p = -(g\hat{z} + \ddot{p}_c) + \lambda_a v_e + \lambda_b p_e + \theta_t \alpha + \theta_t u_1 \delta R\hat{z} \tag{18}$$

where $\delta R = R - R_c$.

- *Assumption 5:* $\theta_t^m \le \theta_t \le \theta_t^u$, with $0 < \theta_t^m, \theta_t^u$ being known *a priori*.

The control input α in (18) is specified as

$$\alpha = \frac{1}{\hat{\theta}_t}\varphi_t \tag{19}$$

where

$$\varphi_t = -k_p z_p - \lambda_a v_e - \lambda_b p_e + g\hat{z} + \ddot{p}_c \tag{20}$$

Based on (16), it is clear that the linear control term $-k_p z_p$ in (20) is actually the PID control in the p_e dynamics. By substituting (19) and (20) into (18), it yields the following closed-loop z_p dynamics

$$\begin{aligned}\dot{z}_p &= -(g\hat{z} + \ddot{p}_c) + \lambda_a v_e + \lambda_b p_e + \varphi_t + (\frac{\theta_t}{\hat{\theta}_t} - 1)\varphi_t \\ &\quad + \theta_t u_1 \delta R\hat{z} \\ &= -k_p z_p + \frac{\tilde{\theta}_t}{\hat{\theta}_t}\varphi_t + \theta_t u_1 \delta R\hat{z}\end{aligned} \tag{21}$$

Compared to the popular Lyapunov-based update algorithm (LBUA), the composite update algorithm generally leads to better tracking performance [26]. In this regard, the following SPIM is introduced [29]

$$\dot{\hat{z}}_p = -(g\hat{z} + \ddot{p}_c) + \lambda_a v_e + \lambda_b p_e + \hat{\theta}_t u_1 R\hat{z} + \beta_p \tilde{z}_p \tag{22}$$

where $\tilde{z}_p = z_p - \hat{z}_p$.

By subtracting (17) from (22), it yields

$$\dot{\tilde{z}}_p = -\beta_p \tilde{z}_p + \tilde{\theta}_t (u_1 R\hat{z}) \tag{23}$$

The following equation is easy to verify and will be used frequently in the upcoming formulation

$$|\tilde{\theta}_t u_1 R\hat{z}| = |\tilde{\theta}_t \frac{\varphi_t}{\hat{\theta}_t}| \tag{24}$$

The composite update algorithm for $\hat{\theta}_t$ is specified as

$$\dot{\hat{\theta}}_t = \mathcal{P}(\eta_t), \tag{25}$$

where

$$\eta_t = \gamma_1 [(1 + \gamma_p \beta_p)\tilde{z}_p^T (u_1 R\hat{z}) - \sigma_1 \hat{\theta}_t] \tag{26}$$

By virtue of P1, it is clear that $\hat{\theta}_t(t)$ lies within $\Omega_t \triangleq \{\hat{\theta}_t | \theta_t^m \le \hat{\theta}_t \le \theta_t^u\}$ for all time once $\hat{\theta}_t(0) \in \Omega_t$.

Remark 2: Even though the thrust factor b can be identified through an off-line static thrust test, however, uncertainty in θ_t may easily arise from changes in the payload, air density, etc., in a real fly [19]. Consequently, it is more practical to consider cases with prior knowledge of the bounding set $[\theta_t^m, \theta_t^u]$ than θ_t itself. Note that such a bounding set is not difficult to determine when a nominal value of θ_t is available.

Using (9) and (19), the desired pitch and roll angles are generated as

$$\begin{aligned}\phi_c &= \sin^{-1}(\frac{s_{\psi_c}\alpha_1 - c_{\psi_c}\alpha_2}{|\alpha|}) \\ \theta_c &= \tan^{-1}(\frac{c_{\psi_c}\alpha_1 + s_{\psi_c}\alpha_2}{\alpha_3})\end{aligned} \tag{27}$$

By replacing ϕ, θ, and ψ in (9) with ϕ_c, θ_c, and ψ_c, the rotation matrix command R_c can be attained immediately.

B. INNER-LOOP DESIGN

The inner-loop control design aims to minimize the destabilizing effect caused by the residual coupling nonlinearity $\theta_t u_1 \delta R\hat{z}$ in (21). Before the start, the bound for $\delta R\hat{z}$ is estimated as

$$\begin{aligned}|\delta R\hat{z}|^2 &= \hat{z}^T(R-R_c)^T(R-R_c)\hat{z}\\ &= 2\hat{z}^T(I-R_e)\hat{z}\\ &\le 2[\hat{x}^T(I-R_e)\hat{x}+\hat{y}^T(I-R_e)\hat{y}+\hat{z}^T(I-R_e)\hat{z}]\end{aligned}$$

where $R_e = R_c^T R$. It follows that

$$|\delta R\hat{z}| \le \sqrt{2tr(I-R_e)} \tag{28}$$

First, the criterion $-1 \le tr(R_e) \le 3$ fulfills since $R_e \in SO(3)$ [1]. Therefore, the bound in (28) is well-defined. Next, based on (2) and (4), the control objective is then equivalent to ensure $\varepsilon = (R_e - R_e^T)^\vee \to 0$ and $0 \le tr(I-R_e) < 4$ for all time. To speed up the convergence, the restriction is set to $0 \le tr(I-R_e) < a$, $0 < a < 4$ in the upcoming derivation.

To begin with, define the following BLF

$$V_b = \ln \frac{a}{a - tr(I-R_e)} \tag{29}$$

Clearly, boundedness of V_b implies that $0 \le tr(I-R_e) < a$, or equivalently, $(1-0.25a) < \cos^2(\xi/2) \le 1.0$ based on (4). Under such circumstances, (28) can be further simplified as

$$|\delta R\hat{z}| \le (\frac{2}{4-a})^{1/2}|\varepsilon| \tag{30}$$

By a direct differentiation of (29), it yields

$$\begin{aligned}\dot{V}_b &= -\frac{tr(\dot{R}_e)}{a-tr(I-R_e)}\\ &= -\frac{tr(R_e\Omega_e^\wedge)}{a-tr(I-R_e)}\end{aligned} \tag{31}$$

where $\Omega_e = \Omega - \Omega_c$ with $\Omega_c = R_e^T(R_c^T\dot{R}_c)^\vee$ [17].

Based on (1), one has

$$\dot{V}_b = \frac{\varepsilon^T\Omega_e}{a-tr(I-R_e)} \tag{32}$$

Note that Ω_c contains the acceleration signals $\dot{v}_e$ embedded in $\dot{R}_c$ and therefore is not directly cancellable. To get this around, the following first-order low-pass filters, i.e., the DSC schemes, are employed herein

$$\begin{aligned}\dot{\phi}_{c,f} &= \beta_0(\phi_c - \phi_{c,f}), \quad \phi_{c,f}(0) = \phi_c(0),\\ \dot{\theta}_{c,f} &= \beta_0(\theta_c - \theta_{c,f}), \quad \theta_{c,f}(0) = \theta_c(0),\end{aligned} \tag{33}$$

where $\beta_0 > 0$ is a constant, $\phi_{c,f}$ and $\theta_{c,f}$ are the outputs of the filters. By replacing $\dot{\phi}_c$ and $\dot{\theta}_c$ in $\dot{R}_c$ with $\dot{\phi}_{c,f}$ and $\dot{\theta}_{c,f}$, a new matrix $\dot{R}_{c,f}$ is generated and will be used as an approximation of $\dot{R}_c$ to resolve the aforementioned difficulty. Its justification will be further clarified later in Remark 3.

Based on (1) and (33), (32) can be rewritten as

$$\begin{aligned}\dot{V}_b &= \frac{\varepsilon^T\Omega_e}{a-tr(I-R_e)}\\ &= \frac{\varepsilon^T(\Omega - \Omega_{c,f} - \delta\Omega_c)}{a-tr(I-R_e)}\end{aligned} \tag{34}$$

where $\Omega_{c,f} = R_e^T(R_c^T\dot{R}_{c,f})^\vee$ and $\delta\Omega_c = \Omega_c - \Omega_{c,f}$.

Note that $\dot{\Omega}_{c,f}$ is also non-cancellable. Therefore, the following DSC scheme is employed again

$$\dot{\Omega}^a_{c,f} = \beta_0(\Omega_{c,f} - \Omega^a_{c,f}), \quad \Omega^a_{c,f}(0) = \Omega_{c,f}(0), \tag{35}$$

where $\Omega^a_{c,f} \in R^3$ is the output of the filter.

Define a new error state z_e

$$z_e = \Omega - \Omega^a_{c,f} - q, \tag{36}$$

where q is the output of the following filter

$$\dot{q} = \beta_0(\alpha_e - q), \quad q(0) = \alpha_e(0), \tag{37}$$

with α_e being the virtual controller to be specified later on.

Equation (34) can be rewritten in terms of z_e as

$$\dot{V}_b = \frac{\varepsilon^T(z_e + \alpha_e - \delta\alpha_e - \delta\Omega_c - \delta\Omega_{c,f})}{a-tr(I-R_e)} \tag{38}$$

where $\delta\alpha_e = \alpha_e - q$ and $\delta\Omega_{c,f} = \Omega_{c,f} - \Omega^a_{c,f}$.

The virtual control α_e is specified as

$$\begin{aligned}\alpha_e = &-k_{b,1}\varepsilon - \frac{k_{b,2}\varepsilon}{a-tr(I-R_e)} - k_{b,3}u_1|z_p|\\ &\cdot (a-tr(I-R_e))\tanh(\frac{k_{b,3}u_1|z_p|\varepsilon}{w_0})\end{aligned} \tag{39}$$

where $k_{b,i}$, $i = 1, 2, 3$ are gain constants.

Remark 3: In the conventional backstepping design, the error state z_e is in a form of

$$z_e = \Omega - \Omega^a_{c,f} - \alpha_e. \tag{40}$$

Due to the direct compensation of the residual coupling nonlinearity in (39), the corresponding z_e dynamics will contain acceleration signals $\dot{v}_e$ and $\dot{z}_p$ arising from $\dot{\alpha}_e$. They may call for extra implementation costs and incur the explosion of complexity problem at the same time [34]. Via introducing the DSC method in (37) and a redefinition of z_e in (36), such a difficulty is alleviated since it is the filtered output q instead of α_e being differentiated [33]. Clearly, to minimize the possible deterioration in tracking performance, the state $q(t)$ should resemble $\alpha_e(t)$ as much as possible, which can be achieved via picking up a big β_0.

Via substituting (39) into (38), it yields

$$\begin{aligned}\dot{V}_b = &-\frac{k_{b,1}|\varepsilon|^2}{a-tr(I-R_e)} - \frac{k_{b,2}|\varepsilon|^2}{(a-tr(I-R_e))^2}\\ &- k_{b,3}u_1|z_p|\varepsilon^T\tanh(\frac{k_{b,3}u_1|z_p|\varepsilon}{w_0})\\ &+ \frac{\varepsilon^T(z_e - \delta\alpha_e - \delta\Omega_c - \delta\Omega_{c,f})}{a-tr(I-R_e)}\end{aligned} \tag{41}$$

On the other hand, by a direct differentiation of z_e in (36), it yields

$$\begin{aligned}\dot{z}_e &= \dot{\Omega} - \dot{\Omega}^a_{c,f} - \dot{q}\\ &= J^{-1}(-\Omega^\wedge J\Omega + \tau) - \dot{\Omega}^a_{c,f} - \dot{q}\\ &= \theta_u .* \bar{u} + Y_r\theta_r - \dot{\Omega}^a_{c,f} - \dot{q}\end{aligned} \tag{42}$$

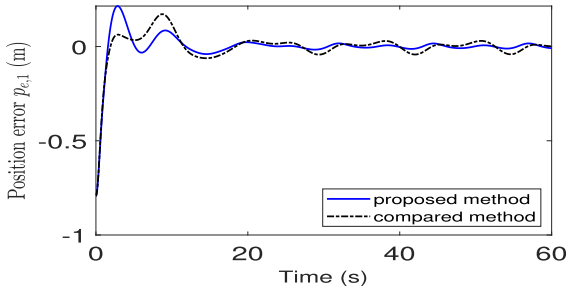

FIGURE 2. Position error $p_{e,1}$.

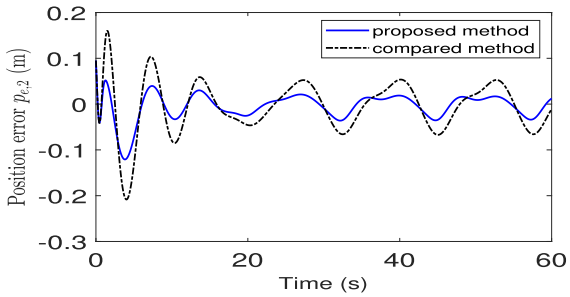

FIGURE 3. Position error $p_{e,2}$.

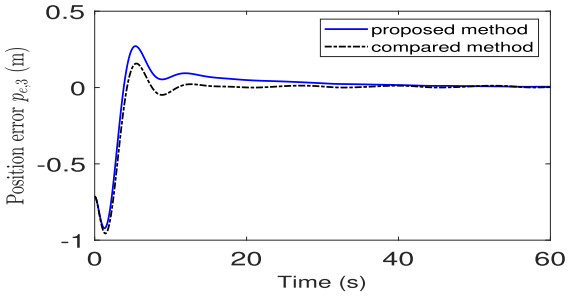

FIGURE 4. Position error $p_{e,3}$.

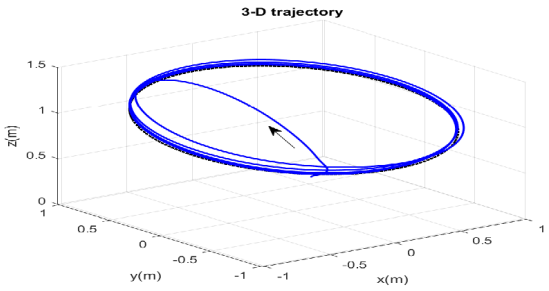

FIGURE 5. Trajectory in 3-D space.

where $\bar{u} = [u_2, u_3, u_4]^T$, $\theta_u = col[\frac{bl}{J_1}, \frac{bl}{J_2}, \frac{\kappa}{J_3}]$, and

$$\theta_r = [\frac{J_y - J_z}{J_x}, \frac{J_z - J_x}{J_y}, \frac{J_x - J_y}{J_z}]^T$$
$$Y_r = \begin{bmatrix} \Omega_y\Omega_z & 0 & 0 \\ 0 & \Omega_x\Omega_z & 0 \\ 0 & 0 & \Omega_x\Omega_y \end{bmatrix} \tag{43}$$

The following control algorithm for $\bar{u}$ is proposed herein,

$$\bar{u} = \hat{\theta}_u^{-1} .* \varphi_r, \tag{44}$$

where $\hat{\theta}_u^{-1} = col[1/\hat{\theta}_{u,1}, 1/\hat{\theta}_{u,2}, 1/\hat{\theta}_{u,3}]$ and

$$\varphi_r = -k_e z_e - Y_r\hat{\theta}_r + \dot{\Omega}^a_{c,f} + \dot{q}, \tag{45}$$

with $k_e > 0$ being a gain constant.

By substituting (45) and (44) into (42), it yields the following closed-loop system

$$\begin{aligned} \dot{z}_e &= -k_e z_e + \tilde{\theta}_u .* \hat{\theta}_u^{-1} .* \varphi_r + Y_r\tilde{\theta}_r \\ &= -k_e z_e + Y\tilde{\vartheta} \end{aligned} \tag{46}$$

where $Y = [Y_u \vdots Y_r]$, $Y_u = diag(\varphi_{r,i}/\hat{\theta}_{u,i})$, $i = 1, 2, 3$, and $\tilde{\vartheta} = \vartheta - \hat{\vartheta}$, with $\vartheta = col[\theta_u, \theta_r]$.

Similarly, to achieve better tracking performance, the following SPIM for estimating $\hat{\vartheta}$ is adopted herein

$$\dot{\hat{z}}_e = \beta_z\tilde{z}_e + Y\hat{\vartheta} - \dot{\Omega}^a_{c,f} - \dot{q}_e, \tag{47}$$

where $\hat{z}_e$ is the estimated state, $\beta_z > 0$ is a gain constant, and $\tilde{z}_e = z_e - \hat{z}_e$.

By subtracting (42) from (47), it yields

$$\dot{\tilde{z}}_e = -\beta_z\tilde{z}_e + Y\tilde{\vartheta} \tag{48}$$

- *Assumption 6:* $\theta^m_{u,i} \le \theta_{u,i} \le \theta^u_{u,i}$, where $i = 1, 2, 3$ and $\theta^m_{u,i}$, $\theta^u_{u,i}$ are known constants.

The composite update algorithm for $\hat{\vartheta}$ is specified as

$$\dot{\hat{\vartheta}} = \eta, \tag{49}$$

where $\eta = col[\mathcal{P}(\eta_u), \eta_r]$, with

$$\begin{aligned} \eta_u &= \gamma_2\{Y_u[z_e + (1 + \gamma_\theta\beta_z)\tilde{z}_e] - \sigma_2\hat{\theta}_u\}, \\ \eta_r &= \gamma_2\{Y_r[z_e + (1 + \gamma_\theta\beta_z)\tilde{z}_e] - \sigma_2\hat{\theta}_r\}, \end{aligned} \tag{50}$$

where $\gamma_2, \gamma_\theta > 0$ being gain constants. Similarly, $\hat{\theta}_u(t)$ lies within $\Omega_u \triangleq \{\hat{\theta}_u | \theta^m_{u,i} \le \hat{\theta}_{u,i} \le \theta^u_{u,i}\}$, $i = 1, 2, 3$ for all time once $\hat{\theta}_u(0) \in \Omega_u$.

Remark 4: By a simple manipulation, (23) and (48) can be rewritten in a singular-perturbation form of

$$\begin{aligned} \frac{1}{\beta_p}\frac{d}{dt}(\beta_p\tilde{z}_p) &= -\beta_p\tilde{z}_p + \tilde{\theta}_t u_1 R\hat{z}, \\ \frac{1}{\beta_z}\frac{d}{dt}(\beta_z\tilde{z}_e) &= -\beta_z\tilde{z}_e + Y\tilde{\vartheta} \end{aligned} \tag{51}$$

Clearly, the subsystems (23), (33), (35), (37), and (48) act as the *fast dynamics* while the rest closed-loop system is the *slow dynamics* when $\beta_0, \beta_p, \beta_z \gg 1$. Under such circumstances, the errors $|\nu_a(t)| = |\beta_p\tilde{z}_p - \tilde{\theta}_t u_1 R\hat{z}|$, $|\nu_b| = |\beta_z\tilde{z}_e - Y\tilde{\vartheta}|$, $|\delta\phi_c| = |\phi_c - \phi_{c,f}|$, $|\delta\theta_c| = |\theta_c - \theta_{c,f}|$, $|\delta\Omega_{c,f}|$, and $|\delta\alpha_e|$ converge exponentially to the set $[0, \epsilon_1]$ within the time interval $[0, T_1]$ and stay there for $t \ge T_1$, where $\epsilon_1, T_1 > 0$ can be made arbitrarily small via using sufficiently big β_0, β_p, and β_z [33].

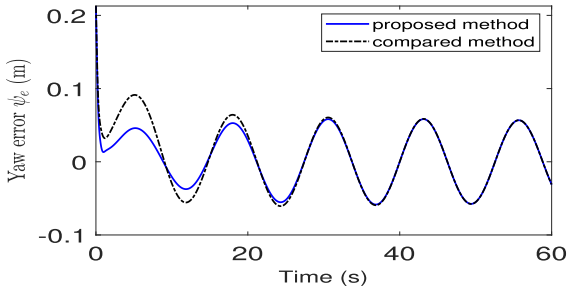

FIGURE 6. Yaw angle error $\psi_e = \psi - \psi_c$.

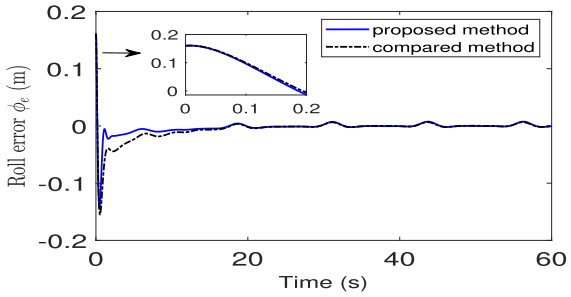

FIGURE 7. Roll angle error $\phi_e = \phi_{c,f} - \phi_c$.

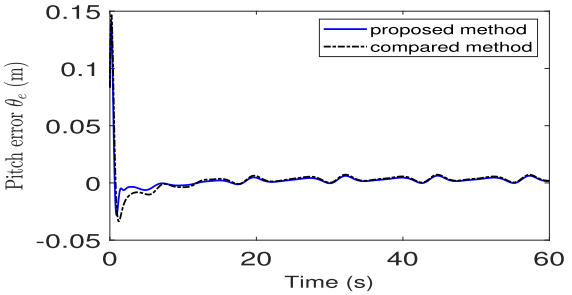

FIGURE 8. Pitch angle error $\theta_e = \theta_{c,f} - \theta_c$.

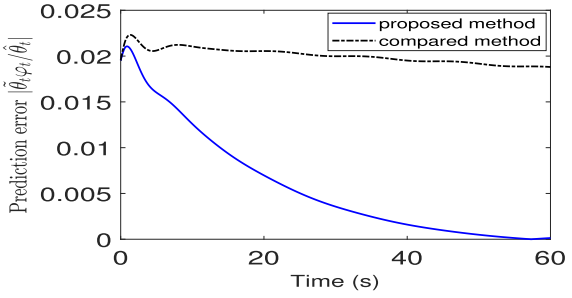

FIGURE 9. Norm of the prediction error $\tilde{\theta}_t\varphi_t/\hat{\theta}_t$.

Remark 5: Via taking Laplace transformation on both sides of (33), we have

$$\phi_{c,f}(s) = \frac{1}{(s/\beta_0)+1}\phi_c(s),$$
$$\theta_{c,f}(s) = \frac{1}{(s/\beta_0)+1}\theta_c(s). \tag{52}$$

Next, by multiplying s to both sides of (52), it yields

$$\dot{\phi}_{c,f}(t) = \frac{1}{(s/\beta_0)+1}\dot{\phi}_c(t),$$
$$\dot{\theta}_{c,f}(t) = \frac{1}{(s/\beta_0)+1}\dot{\theta}_c(t), \tag{53}$$

which implies that $|\delta\dot{\phi}_c| = |\dot{\phi}_c - \dot{\phi}_{c,f}|$ and $|\delta\dot{\theta}_c| = |\dot{\theta}_c - \dot{\theta}_{c,f}|$ will also converge to $[0, \epsilon_1]$ within $[0, T_1]$. It can then be expected that $|\delta\dot{R}_c| = |\dot{R}_c - \dot{R}_{c,f}| = |(\partial R_c/\partial\phi_c)\delta\dot{\phi}_c + (\partial R_c/\partial\theta_c)\delta\dot{\theta}_c|$ will be $\mathcal{O}(\epsilon_1)$ for all $t \geq T_1$. As a consequence, $|\delta\Omega_c|$ will also converge to $[0, \epsilon_1]$ within $[0, T_1]$ after a reselection of T_1.

Define

$$\begin{aligned}
k_a &= \min[2k_p - 1, 2\beta_p, \gamma_1\sigma_1, (4-a)k_{b,1}, 2k_e - 1, \\
&\qquad 2\beta_z, \gamma_2\sigma_2] \\
\gamma_a &= \min(\gamma_p - \frac{1}{\theta_t}, \gamma_\theta) \\
\delta_a &= (\gamma_p + \gamma_\theta + 3)\epsilon_1^2 + \sigma_1|\theta_t|^2 + \sigma_2|\vartheta|^2 + 6c_\varsigma w_0 \\
k_b &= \min[2k_p - 1, (4-a)k_{b,1}, 2k_e - 2] \\
\delta_b &= (1+c_1)\delta_a/\gamma_a + 3\epsilon_1^2 + 6c_\varsigma w_0
\end{aligned} \tag{54}$$

The main results are summarized in the following.

Theorem 1: Consider the closed-loop system, consisting of the system dynamics in (8), the virtual/actual controllers in (19), (39), (44), and the update algorithms in (25) and (49). For any bounded initial states fulfilling $\hat{\theta}_t(0) \in [\theta_t^m, \theta_t^u]$, $\hat{\theta}_{u,i}(0) \in [\theta_{u,i}^m, \theta_{u,i}^u]$, $i = 1, 2, 3$, and $tr(I - R_e(0)) < a$, the following properties hold when $k_a, k_b, \gamma_a > 0$, $k_{b,2} \geq 2$, and $k_{b,3} \geq (2/(4-a))^{1/2}$.

F1) All the signals in the closed-loop system remain bounded for all time.

F2) $tr(I - R_e(t)) < a, \forall t \geq 0$.

F3) There exists a finite positive number T_a such that

$$[|\tilde{\theta}_t\frac{\varphi_t}{\hat{\theta}_t}|^2 + |Y\tilde{\vartheta}|^2]^{1/2} \leq \sqrt{\frac{(1+c_1)\delta_a}{\gamma_a}}, \tag{55}$$

$\forall t \geq T_a$, and $0 < c_1 < 1$ is an arbitrary constant.

F4) The tracking error $z_p(t)$ is ultimately bounded by

$$|z_p| \leq \sqrt{\frac{(1+c_2)\theta_t\delta_b}{k_b}}, \quad \forall t \geq T_b, \tag{56}$$

where $0 < c_2 < 1$ and $T_b \geq T_a$ is a positive number.

Proof: Select the following Lyapunov function

$$\begin{aligned}
V_1(t) = \frac{1}{2}(&\frac{1}{\theta_t}z_p^T z_p + \tilde{z}_p^T\tilde{z}_p + \frac{1}{\gamma_1}\tilde{\theta}_t^2 + z_e^T z_e \\
&+ \tilde{z}_e^T\tilde{z}_e + \frac{1}{\gamma_2}\tilde{\vartheta}^T\tilde{\vartheta}) + V_b
\end{aligned} \tag{57}$$

The time derivative of $V_1(t)$ along (21), (23), (25), (41), (46), (48), and (49) can be calculated as follows

$$\dot{V}_1(t) = \frac{1}{\theta_t}z_p^T\dot{z}_p + \tilde{z}_p^T\dot{\tilde{z}}_p - \frac{1}{\gamma_1}\tilde{\theta}_t\dot{\hat{\theta}}_t + \dot{V}_b$$

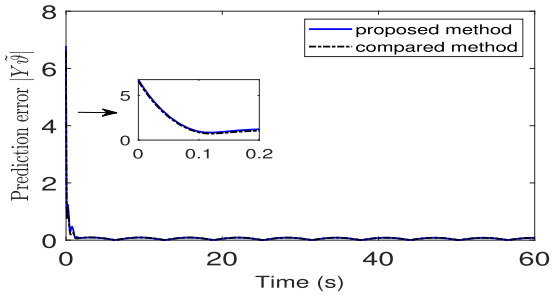

FIGURE 10. Norm of the prediction error $Y\tilde{\vartheta}$.

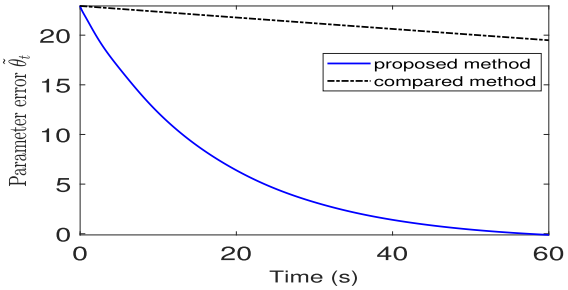

FIGURE 11. Parameter error $\tilde{\theta}_t$.

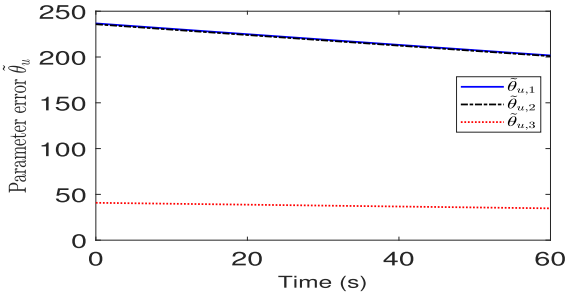

FIGURE 12. Parameter error vector $\tilde{\theta}_u$.

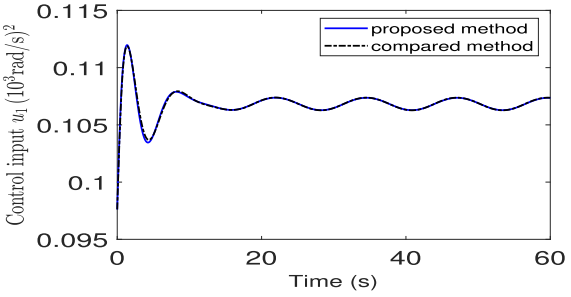

FIGURE 13. Control input u_1.

$$
\begin{aligned}
&+ z_e^T\dot{z}_e + \tilde{z}_e^T\dot{\tilde{z}}_e - \frac{1}{\gamma_2}\tilde{\vartheta}^T\dot{\hat{\vartheta}} \\
&= \frac{1}{\theta_t}(-k_p z_p^T z_p + \frac{\tilde{\theta}_t}{\hat{\theta}_t} z_p^T\varphi_t) + u_1 z_p^T\delta R\hat{z} \\
&+ \tilde{z}_p^T(-\beta_p\tilde{z}_p + \tilde{\theta}_t u_1 R\hat{z}) - \tilde{\theta}_t\mathcal{P}(\eta_t) \\
&- \frac{k_{b,1}|\varepsilon|^2}{a - tr(I - R_e)} - \frac{k_{b,2}|\varepsilon|^2}{(a - tr(I - R_e))^2} \\
&- k_{b,3}u_1|z_p|\varepsilon^T\tanh(\frac{k_{b,3}u_1|z_p|\varepsilon}{w_0}) \\
&+ \frac{\varepsilon^T(z_e - \delta\alpha_e - \delta\Omega_c - \delta\Omega_{c,f})}{a - tr(I - R_e)} - \tilde{\vartheta}^T\eta \\
&+ z_e^T(-k_e z_e + Y\tilde{\vartheta}) + \tilde{z}_e^T(-\beta_z\tilde{z}_e + Y\tilde{\vartheta}) \qquad (58)
\end{aligned}
$$

By including $\theta_t^{-1}z_p^T z_p$ instead of the standard $z_p^T z_p$ into (57), the required gain $k_{b,3}$ is significantly reduced when θ_t is with a high value, e.g, the typical value of $\theta_t = 91.76$ in the subsequent Section IV. The price is that the prediction error term $\theta_t^{-1}\tilde{\theta}_t\varphi_t/\hat{\theta}_t$ cannot be directly canceled. By using the modular update algorithm in (25), such a difficulty is circumvented with ease [12].

By completing the squares, one has

$$
\begin{aligned}
\theta_t^{-1}(\tilde{\theta}_t\frac{z_p^T\varphi_t}{\hat{\theta}_t}) &\le \frac{1}{2}\theta_t^{-1}(|\frac{\tilde{\theta}_t\varphi_t}{\hat{\theta}_t}|^2 + |z_p|^2) \\
\frac{\varepsilon^T z_e}{a - tr(I - R_e)} &\le \frac{1}{2}(\frac{|\varepsilon|^2}{(a - tr(I - R_e))^2} + |z_e|^2) \\
\frac{-\varepsilon^T(\delta\alpha_e)}{a - tr(I - R_e)} &\le \frac{1}{2}(\frac{|\varepsilon|^2}{(a - tr(I - R_e))^2} + |\delta\alpha_e|^2) \\
\frac{-\varepsilon^T(\delta\Omega_c)}{a - tr(I - R_e)} &\le \frac{1}{2}(\frac{|\varepsilon|^2}{(a - tr(I - R_e))^2} + |\delta\Omega_c|^2)
\end{aligned}
$$

$$
\frac{-\varepsilon^T(\delta\Omega_{c,f})}{a - tr(I - R_e)} \le \frac{1}{2}(\frac{|\varepsilon|^2}{(a - tr(I - R_e))^2} + |\delta\Omega_{c,f}|^2) \qquad (59)
$$

Next, by substituting (59) into (58), then cancelling out the indefinite terms $\tilde{\theta}_t(u_1\tilde{z}_p^T R\hat{z})$, $(z_e + +\tilde{z}_e)^T Y\tilde{\vartheta}$ based on P2, it yields

$$
\begin{aligned}
\dot{V}_1(t) \le \frac{1}{\theta_t}[-(k_p - \frac{1}{2})|z_p|^2 + \frac{1}{2}|\frac{\tilde{\theta}_t\varphi_t}{\hat{\theta}_t}|^2] + u_1 z_p^T\delta R\hat{z} \\
- \beta_p|\tilde{z}_p|^2 - \frac{k_{b,1}|\varepsilon|^2}{a - tr(I - R_e)} - \frac{(k_{b,2} - 2)|\varepsilon|^2}{(a - tr(I - R_e))^2} \\
- k_{b,3}u_1|z_p|\varepsilon^T\tanh(\frac{k_{b,3}u_1|z_p|\varepsilon}{w_0}) - (k_e - \frac{1}{2})|z_e|^2 \\
- \tilde{\theta}_t(\gamma_p\beta_p\tilde{z}_p^T(u_1 R\hat{z}) - \sigma_1\hat{\theta}_t) - \beta_z\tilde{z}_e^T\tilde{z}_e \\
- \tilde{\vartheta}^T(\gamma_\theta\beta_z Y^T\tilde{z}_e - \sigma_2\hat{\vartheta}) + \frac{1}{2}(|\delta\alpha_e|^2 + |\delta\Omega_c|^2 \\
+ |\delta\Omega_{c,f}|^2) \qquad (60)
\end{aligned}
$$

By recalling (24) and completing the squares again, we have

$$
\begin{aligned}
-\gamma_p\beta_p\tilde{\theta}_t\tilde{z}_p^T(u_1 R\hat{z}) &= -\gamma_p(v_a + \tilde{\theta}_t u_1 R\hat{z})^T(\tilde{\theta}_t u_1 R\hat{z}) \\
&\le \frac{\gamma_p}{2}(-|\tilde{\theta}_t u_1 R\hat{z}|^2 + |v_a|^2) \\
&= \frac{\gamma_p}{2}(-|\tilde{\theta}_t\frac{\varphi_t}{\hat{\theta}_t}|^2 + |v_a|^2) \\
-\gamma_\theta\beta_z\tilde{\vartheta}^T Y^T\tilde{z}_e &= -\gamma_\theta(Y\tilde{\vartheta})^T(v_b + Y\tilde{\vartheta}) \\
&\le \frac{\gamma_\theta}{2}(-|Y\tilde{\vartheta}|^2 + |v_b|^2) \\
\sigma_1\tilde{\theta}_t\hat{\theta}_t &\le \frac{\sigma_1}{2}(-\tilde{\theta}_t^2 + \theta_t^2),
\end{aligned}
$$

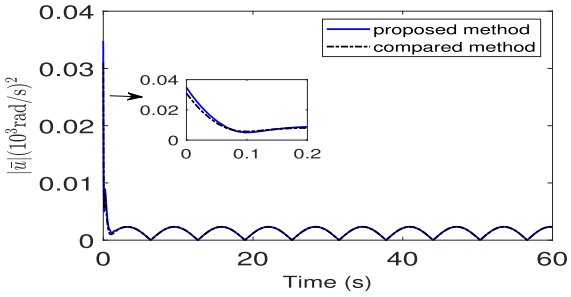

FIGURE 14. Norm of the control input vector $\bar{u}$.

$$\sigma_2 \tilde{\vartheta}^T \hat{\vartheta} \leq \frac{\sigma_2}{2}(-\tilde{\vartheta}^T \tilde{\vartheta} + \vartheta^T \vartheta) \tag{61}$$

The following result can be easily inferred based on (30)

$$\begin{aligned} & u_1 z_p^T \delta R \hat{z} - k_{b,3} u_1 |z_p| \varepsilon^T \tanh(\frac{k_{b,3} u_1 |z_p| \varepsilon}{w_0}) \\ & \leq (\frac{2}{4-a})^{1/2} u_1 |z_p| |\varepsilon|_1 - k_{b,3} u_1 |z_p| \\ & \quad \cdot \varepsilon^T \tanh(\frac{k_{b,3} u_1 |z_p| \varepsilon}{w_0}) \leq 3 c_\varsigma w_0 \end{aligned} \tag{62}$$

Based on (2) and (5), it can be easily seen that

$$\begin{aligned} & -\frac{k_{b,1}|\varepsilon|^2}{a - tr(I - R_e)} \\ & = -4 k_{b,1} \cos^2 \frac{\xi}{2} \frac{tr(I - R_e)}{a - tr(I - R_e)} \\ & \leq -4 k_{b,1} (1 - \frac{a}{4}) \ln \frac{a}{a - tr(I - R_e)} \\ & \leq -(4 - a) k_{b,1} V_b \end{aligned} \tag{63}$$

Substituting (62)-(63) into (60), it yields

$$\begin{aligned} \dot{V}_1 \leq & -k_a V_1 - \frac{\gamma_a}{2}(|\tilde{\theta}_t \frac{\varphi_t}{\hat{\theta}_t}|^2 + |Y \tilde{\vartheta}|^2) \\ & + \frac{1}{2}[\gamma_p |\nu_a|^2 + \gamma_\theta |\nu_b|^2 + |\delta \alpha_e|^2 + |\delta \Omega_c|^2 \\ & + |\delta \Omega_{c,f}|^2 + \sigma_1 |\theta_t|^2 + \sigma_2 |\vartheta|^2] + 3 c_\varsigma w_0 \end{aligned} \tag{64}$$

As explained in Remark 4, given $\epsilon_1 > 0$, there exist $0 < T_1$ and sufficiently big $\beta_0, \beta_p, \beta_z$, such that the errors $|\nu_a(t)|$, $|\nu_b(t)|$, $|\delta \alpha_e(t)|$, $|\delta \Omega_c(t)|$, and $|\delta \Omega_{c,f}(t)|$ converge exponentially to the set $[0, \epsilon_1]$ within the time interval $[0, T_1]$ and stay there for $t \geq T_1$. As a result, (64) can be rewritten as

$$\dot{V}_1 \leq -k_a V_1 - \frac{\gamma_a}{2}[|\tilde{\theta}_t \frac{\varphi_t}{\hat{\theta}_t}|^2 + |Y \tilde{\vartheta}|^2] + \frac{\delta_a}{2} \tag{65}$$

for all $t \geq T_1$. Clearly, F1 and hence F2 sustain immediately.

Define

$$\begin{aligned} \varrho(t) = \max\{0, (2k_a)^{-1}[(1 + c_1)\delta_a \\ - \gamma_a(|\tilde{\theta}_t \frac{\varphi_t}{\hat{\theta}_t}|^2 + |Y \tilde{\vartheta}|^2)]\} \end{aligned} \tag{66}$$

It is not hard to see that $0 \leq \varrho(t) \leq (1 + c_1)\delta_a/(2k_a)$. By adding and subtracting $k_a \varrho(t)$ to the righthand side of (64), it becomes

$$\dot{V}_1 \leq -k_a(V_1 - \varrho(t)) - \frac{c_1 \delta_a}{2} \tag{67}$$

TABLE 1. Numerical values of model parameters.

Symbol	Value	Unit
J	$[0.0259, 0.0260, 0.0397]^T$	$kg \cdot m^2$
m	1.336	kg
l	0.2	m
b	122.6	$N/(10^3 rad/s)^2$
κ	6.48	$N \cdot m/(10^3 rad/s)^2$

Since $\dot{V}_1 \leq -c_1 \delta_a/2$ whenever $V_1 \geq \varrho(t)$, consequently, there always exists a constant $T_a > 0$ such that $V_1 \leq \varrho(t), \forall t \geq T_a$, which in turn implies that $\gamma_a(|\tilde{\theta}_t \varphi_t / \hat{\theta}_t|^2 + |Y \tilde{\vartheta}|^2) \leq (1 + c_1)\delta_a/2, \forall t \geq T_a$. Property F3 is thus proven.

Finally, define the second Lyapunov function $V_2 = (1/2)(\theta_t^{-1} z_p^T z_p + z_e^T z_e) + V_b$. Its time derivative can be calculated as

$$\begin{aligned} \dot{V}_2(t) = & \frac{1}{\theta_t}(-k_p z_p^T z_p + \frac{\tilde{\theta}_t}{\hat{\theta}_t} z_p^T \varphi_t) + u_1 z_p^T \delta R \hat{z} \\ & - \frac{k_{b,1}|\varepsilon|^2}{a - tr(I - R_e)} - \frac{k_{b,2}|\varepsilon|^2}{(a - tr(I - R_e))^2} \\ & - k_{b,3} u_1 |z_p| \varepsilon^T \tanh(\frac{k_{b,3} u_1 |z_p| \varepsilon}{w_0}) \\ & + \frac{\varepsilon^T (z_e - \delta \alpha_e - \delta \Omega_c - \delta \Omega_{c,f})}{a - tr(I - R_e)} \\ & + z_e^T(-k_e z_e + Y \tilde{\vartheta}) \end{aligned} \tag{68}$$

By invoking (62)-(63) and F3, after some straightforward manipulations, it yields

$$\dot{V}_2 \leq -k_b V_2 + \frac{\delta_b}{2}, \quad \forall t \geq T_b \tag{69}$$

The property F4 can then be inferred immediately. ■

Remark 6: The major advantages of the proposed design are twofold, the direct compensation of the coupling nonlinearity $\theta_t u_1 \delta R$ and the SPIM-based update algorithm. Without the former, high control gains are required for ensuring the stability of the closed-loop system. Without the latter, on the other hand, it can be seen from (65) that z_p will be ultimately bounded by

$$|z_p(t)| \leq \sqrt{\frac{(1 + c_2)\theta_t \delta_a'}{k_a'}}, \quad \forall t \geq T_b \tag{70}$$

where $k_a' = \min[2k_p - 1, (4 - a)k_{b,1}, 2k_e - 1, \gamma_1 \sigma_1, \gamma_2 \sigma_2]$ and $\delta_a' = 3\epsilon_1^2 + \sigma_1 |\theta_t|^2 + \sigma_2 |\vartheta|^2 + 6 c_\varsigma w_0$.

To decrease the error bound in (70), the gain k_a' has to be tuned big, which in turn may lead to poor transients or even high-adaptation instability when $\gamma_1 \sigma_1, \gamma_2 \sigma_2 \gg 1$ [25]. In contrast, the proposed SPIM improves the tracking performances in two ways

- The error bound in (56) can be decreased via solely using a big k_b, i.e., big control gains k_p, $k_{b,1}$ and k_e, without big adaptation gains $\gamma_1 \sigma_1$, $\gamma_2 \sigma_2$. The transient performance is therefore improved.
- Via increasing the gain constants γ_p and γ_θ of the SPIM, δ_b and hence the error bound in (56) will be decreased.

The steady-state tracking performance is improved at the same time.

IV. SIMULATION

Note first that the proposed design reduces to the standard TSS approach with LBUA when $k_{b,3} = 0$, $\eta_t = \gamma_1[(z_p^T\varphi_t/\hat{\theta}_t) - \sigma_1\hat{\theta}_t]$, $\eta_u = \gamma_2(Y_u z_e - \sigma_2\hat{\theta}_u)$, and

$$\eta_r = \gamma_2(Y_r z_e - \sigma_2\hat{\theta}_r). \tag{71}$$

A comparative numerical study between these two schemes will be conducted herein to highlight the major advantages of the former.

The adopted model parameters are shown in Table 1. To facilitate the computation, the rotary speeds $\omega_i, i = 1, \cdots, 4$ are in the unit of $10^3 rad/s$. For consistency, the units for the parameters b and κ in Table 1 are $N/(10^3 rad/s)^2$ and $N \cdot m/(10^3 rad/s)^2$, respectively. The reference trajectory is $p_c = [1.0\cos(0.5t), 1.0\sin(0.5t), 1.0 + 0.2\sin(0.5t)]^T$ and $\psi_c = 1.5\sin(0.5\,t)$. The adopted numerical values are: $\lambda_a = 1.0$, $\lambda_b = 1.0$, $k_p = 1.0$, $\gamma_1 = \gamma_2 = 0.5$, $\gamma_p = \gamma_\theta = 10.0$, $\sigma_i = 0.001, i = 1, \cdots, 4$, $\beta_p = \beta_z = 5.0$, $k_{b,1} = k_{b,3} = 1.0$, $k_e = 0.2$, $k_{b,2} = 2.0$, $\theta_t^m = 0.5\theta_t$, $\theta_t^u = 2.0\theta_t$, $\theta_u^m = 0.5\theta_u$, $\theta_u^u = 2.0\theta_u$, and $w_0 = 0.2$, $\beta_0 = 0.1$. The initial states are randomly chosen from [0, 0.3] except that $\hat{\theta}_t(0)$ and $\hat{\theta}_u(0)$ are taken from $[\theta_t^m, \theta_t^u]$ and $[\theta_u^m, \theta_u^u]$, respectively.

The tracking errors $p_e(t)$ and $\psi_e(t)$ of the aforementioned two methods are depicted in Figs. 2-6. Clearly, the proposed design exhibits better tracking performance than the latter. The roll and the pitch angle errors, i.e, $\phi_e(t)$ and $\theta_e(t)$, are kept small after a few seconds of transients, as depicted in Figs. 7-8. The convergence of prediction errors in Figs. 9-10 highlights the major advantages of incorporating SPIM-based update algorithm as stated in Remark 6. Such advantages and the corresponding performance improvement, as stated previously, do not rely on the parameter convergence, as can be seen in Figs. 11-12. Noticeably, the aforementioned achievements do not resort to excessive control efforts as depicted in Figs. 13-14, which further demonstrate its practical applicability.

V. CONCLUDING REMARKS

Using the motors's speeds as the control inputs, this article proposes a robust adaptive tracking controller for quadrotors with parametric uncertainty including the thrust and the drag factors. The residual coupling nonlinearity is directly compensated instead of using the TSS or passivity features of the system. Moreover, the introduced SPIM-based update algorithm ensures the convergence of prediction errors without relying on parameter convergence, which in turn improves the tracking performance. Simulation works demonstrate its effectiveness and practical applicability.

For the future works, in addition to topics like observer-based control [38], [39], reinforcement learning control [40], [41], state/output formation control of multiple quadrotors subjected to parameter uncertainties, external disturbances, communication quantization errors, partially known external reference signals, prescribed performance, etc., is of particular interests (see [42], [43], [44], [45], [46], [47] and references therein). Despite their achievements, however, most of these works used the thrust force and motor torques as control inputs and rely on TSS method incorporating the LBUA for parameter estimation. As can be expected, extension of the proposed design to these tasks would yield better tracking performance and is therefore under our investigation.

ACKNOWLEDGMENT

The authors would like to thank the Editor, an Associate Editor, and the reviewers for their insightful comments, which significantly improve the presentation of the paper.

REFERENCES

[1] R. M. Murray, Z. Li, and S. S. Sastry, *A Mathematical Introduction to Robotic Manipulation*. Boca Raton, FL, USA: CRC Press, 1994, pp. 19–58.
[2] R. W. Prouty, *Helicopter Performance, Stability and Control*. Melbourne, FL, USA: Krieger, 1995, pp. 541–605.
[3] T. Lee, "Exponential stability of an attitude tracking control system on SO(3) for large-angle rotational maneuvers," *Syst. Control Lett.*, vol. 61, no. 1, pp. 231–237, 2012.
[4] T. Lee, M. Leok, and N. H. McClamroch, "Nonlinear robust tracking control of a quadrotor UAV on SE(3)," *Asian J. Control*, vol. 15, no. 2, pp. 391–408, 2013.
[5] A. Tayebi and S. McGilvray, "Attitude stabilization of a VTOL quadrotor aircraft," *IEEE Trans. Control Syst. Technol.*, vol. 14, no. 3, pp. 562–571, May 2006.
[6] Y.-R. Tang, X. Xiao, and Y. Li, "Nonlinear dynamic modeling and hybrid control design with dynamic compensator for a small-scale UAV quadrotor," *Measurement*, vol. 109, pp. 51–64, Oct. 2017.
[7] L. Wang and J. Su, "Switching control of attitude tracking on a quadrotor UAV for large-angle rotational maneuvers," in *Proc. IEEE Int. Conf. Robot. Autom. (ICRA)*, Hong Kong, May 2014, pp. 2907–2912.
[8] J. Zhao, H. Zhang, and X. Li, "Active disturbance rejection switching control of quadrotor based on robust differentiator," *Syst. Sci. Control Eng.*, vol. 8, no. 1, pp. 605–617, Dec. 2020.
[9] X. Shao, X. Yue, and J. Li, "Event-triggered robust control for quadrotors with preassigned time performance constraints," *Appl. Math. Comput.*, vol. 392, Mar. 2021, Art. no. 125667.
[10] S. I. Abdelmaksoud, M. Mailah, and A. M. Abdallah, "Control strategies and novel techniques for autonomous rotorcraft unmanned aerial vehicles: A review," *IEEE Access*, vol. 8, pp. 195142–195169, 2020.
[11] B. J. Emran and H. Najjaran, "A review of quadrotor: An underactuated mechanical system," *Annu. Rev. Control*, vol. 46, pp. 165–180, Jan. 2018.
[12] M. Krstić, I. Kanellakopoulos, and P. V. Kokotović, *Nonlinear and Adaptive Control Design*. New York, NY, USA: Wiley, 1995, pp. 29–64.
[13] W. Dong, J. A. Farrell, M. M. Polycarpou, V. Djapic, and M. Sharma, "Command filtered adaptive backstepping," *IEEE Trans. Control Syst. Technol.*, vol. 20, no. 3, pp. 566–580, May 2012.
[14] J. Zhang, D. Gu, C. Deng, and B. Wen, "Robust and adaptive backstepping control for hexacopter UAVs," *IEEE Access*, vol. 7, pp. 163502–163514, 2019.
[15] T. Hamel, R. Mahony, R. Lozano, and J. Ostrowski, "Dynamic modeling and configuration stabilization for an Xa-flyer," in *Proc. 15th IFAC World Congr.*, Barcelona, Spain, Jul. 2002, pp. 217–222.
[16] S. Bertrand, N. Guénard, T. Hamel, H. Piet-Lahanier, and L. Eck, "A hierarchical controller for miniature VTOL UAVs: Design and stability analysis using singular perturbation theory," *Control Eng. Pract.*, vol. 19, no. 10, pp. 1099–1108, 2011.
[17] Y. Zou, "Nonlinear hierarchical control for quad-rotors with rotation matrix," *Int. J. Control*, vol. 90, no. 7, pp. 1308–1318, Jul. 2017.
[18] H. K. Khalil, *Nonlinear Control*. Upper Saddle River, NJ, USA: Prentice-Hall, 2015, pp. 589–623.

[19] Y. Chen and N. O. Perez-Arancibia, "Adaptive control of aerobatic quadrotor maneuvers in the presence of propeller-aerodynamic-coefficient and torque-latency time-variations," in *Proc. Int. Conf. Robot. Autom. (ICRA)*, Montreal, QC, Canada, May 2019, pp. 6447–6453.

[20] J. Hu and H. Zhang, "Immersion and invariance based command-filtered adaptive backstepping control of VTOL vehicles," *Automatica*, vol. 49, no. 7, pp. 2160–2167, 2013.

[21] B. Zhao, B. Xian, Y. Zhang, and X. Zhang, "Nonlinear robust adaptive tracking control of a quadrotor UAV via immersion and invariance methodology," *IEEE Trans. Ind. Electron.*, vol. 62, no. 5, pp. 2891–2902, May 2015.

[22] S. Islam, P. X. Liu, and A. E. Saddik, "Nonlinear adaptive control for quadrotor flying vehicle," *Nonlinear Dyn.*, vol. 78, no. 1, pp. 117–133, 2014.

[23] Z. Zuo, "Trajectory tracking control design with command-filtered compensation for a quadrotor," *IET Control Theory Appl.*, vol. 4, no. 11, pp. 2343–2355, Nov. 2010.

[24] Y. Zou and Z. Meng, "Immersion and invariance-based adaptive controller for quadrotor systems," *IEEE Trans. Syst., Man Cybern., Syst.*, vol. 49, no. 11, pp. 2288–2297, Nov. 2019.

[25] T. E. Gibson, A. M. Annaswamy, and E. Lavretsky, "On adaptive control with closed-loop reference models: Transients, oscillations, and peaking," *IEEE Access*, vol. 1, pp. 703–717, 2013.

[26] T. Jiang, J. Huang, and B. Li, "Composite adaptive finite-time control for quadrotors via prescribed performance," *J. Franklin Inst.*, vol. 357, no. 10, pp. 5878–5901, Jul. 2020.

[27] Z. T. Dydek, A. M. Annaswamy, and E. Lavretsky, "Adaptive control of quadrotor UAVs: A design trade study with flight evaluations," *IEEE Trans. Control Syst. Technol.*, vol. 21, no. 4, pp. 1400–1406, Jul. 2013.

[28] X. Shao, Q. Hu, D. Li, Y. Shi, and B. Yi, "Composite adaptive control for anti-unwinding attitude maneuvers: An exponential stability result without persistent excitation," *IEEE Trans. Aerosp. Electron. Syst.*, early access, Jul. 29, 2022, doi: 10.1109/TAES.2022.3194846.

[29] K. Guo and Y. Pan, "Composite adaptation and learning for robot control: A survey," *Annu. Rev. Control*, Dec. 2022, doi: 10.1016/j.arcontrol.2022.12.001.

[30] Y. Pan and H. Yu, "Composite learning from adaptive dynamic surface control," *IEEE Trans. Autom. Control*, vol. 61, no. 9, pp. 2603–2609, Sep. 2016.

[31] Q. Hou and J. Dong, "Cooperative output regulation of linear multiagent systems with parameter convergence," *IEEE Trans. Syst., Man, Cybern. Syst.*, vol. 53, no. 1, pp. 518–528, Jan. 2023.

[32] J.-T. Huang and Y.-W. Jiang, "Robust composite adaptive control of linearisable systems with improved performance," *IEEE Access*, vol. 9, pp. 88037–88047, 2021.

[33] J. A. Farrell, M. Polycarpou, M. Sharma, and W. Dong, "Command filtered backstepping," *IEEE Trans. Autom. Control*, vol. 54, no. 6, pp. 1391–1395, Jun. 2009.

[34] J.-T. Huang, "Adaptive fuzzy state/output feedback control of nonstrict-feedback systems: A direct compensation approach," *IEEE Trans. Cybern.*, vol. 49, no. 6, pp. 2046–2059, Jun. 2019.

[35] M. M. Polycarpou, "Stable adaptive neural control schemes for nonlinear systems," *IEEE Trans. Automat. Control*, vol. 41, no. 1, pp. 447–451, Mar. 1996.

[36] X. Huo, M. Huo, and H. R. Karimi, "Attitude stabilization control of a quadrotor UAV by using backstepping approach," *Math. Problems Eng.*, vol. 2014, pp. 1–9, 2014.

[37] N. Wang, S.-F. Su, M. Han, and W.-H. Chen, "Backpropagating constraints-based trajectory tracking control of a quadrotor with constrained actuator dynamics and complex unknowns," *IEEE Trans. Syst., Man, Cybern. Syst.*, vol. 49, no. 7, pp. 1322–1337, Jul. 2019.

[38] X. Shao, J. Liu, H. Cao, C. Shen, and H. Wang, "Robust dynamic surface trajectory tracking control for a quadrotor UAV via extended state observer," *Int. J. Robust Nonlinear Control*, vol. 28, no. 7, pp. 2700–2719, 2018.

[39] H. Hua, Y. Fang, X. Zhang, and B. Lu, "A novel robust observer-based nonlinear trajectory tracking control strategy for quadrotors," *IEEE Trans. Control Syst. Technol.*, vol. 29, no. 5, pp. 1952–1963, Sep. 2021.

[40] X. Lin, Y. Yu, and C.-Y. Sun, "Supplementary reinforcement learning controller designed for quadrotor UAVs," *IEEE Access*, vol. 7, pp. 26422–26431, 2019.

[41] Z. Yao, X. Liang, G.-P. Jiang, and J. Yao, "Model-based reinforcement learning control of electrohydraulic position servo systems," *IEEE/ASME Trans. Mechatronics*, early access, Nov. 18, 2022, doi: 10.1109/TMECH.2022.3219115.

[42] H. Du, W. Zhu, G. Wen, Z. Duan, and J. Lu, "Distributed formation control of multiple quadrotor aircraft based on nonsmooth consensus algorithms," *IEEE Trans. Cybern.*, vol. 49, no. 1, pp. 342–353, Jan. 2019.

[43] X.-Z. Jin, W.-W. Che, Z.-G. Wu, and C. Deng, "Robust adaptive general formation control of a class of networked quadrotor aircraft," *IEEE Trans. Syst., Man, Cybern. Syst.*, vol. 52, no. 12, pp. 7714–7726, Dec. 2022.

[44] X. Huang and J. Dong, "Reliable leader-to-follower formation control of multiagent systems under communication quantization and attacks," *IEEE Trans. Syst., Man, Cybern. Syst.*, vol. 50, no. 1, pp. 89–99, Jan. 2020.

[45] Q. Hou and J. Dong, "Cooperative fault-tolerant output regulation of linear heterogeneous multiagent systems via an adaptive dynamic event-triggered mechanism," *IEEE Trans. Cybern.*, early access, Sep. 23, 2022, doi: 10.1109/TCYB.2022.3204119.

[46] L. Zhang, W.-W. Che, B. Chen, and C. Lin, "Adaptive fuzzy output-feedback consensus tracking control of nonlinear multiagent systems in prescribed performance," *IEEE Trans. Cybern.*, vol. 53, no. 3, pp. 1932–1943, Mar. 2023, doi: 10.1109/TCYB.2022.3171239.

[47] L. Zhang, W.-W. Che, C. Deng, and Z.-G. Wu, "Prescribed performance control for multiagent systems via fuzzy adaptive event-triggered strategy," *IEEE Trans. Fuzzy Syst.*, vol. 30, no. 12, pp. 5078–5090, Dec. 2022.

JENG-TZE HUANG (Senior Member, IEEE) was born in Taichung, Taiwan. He received the B.Sc. degree in mechanical engineering from National Central University, Taiwan, in 1984, the M.S. degree in electrical engineering from National Taiwan University, Taiwan, in 1986, and the Ph.D. degree in electrical and control engineering from National Chiao Tung University, Taiwan, in 1998. He was with the Department of Electronic Engineering, Vanung University, Taiwan, from 1990 to 2007. He was with the Institute of Digital Mechatronic Technology, Chinese Culture University, Taipei, as the Institute Director, from 2011 to 2016, where he is currently a Professor. His current research interests include nonlinear control, adaptive control, intelligent control, and robotics.

YU-WEI JIANG was born in Keelung, Taiwan, in 1999. He received the B.S. degree in mechanical engineering from Chinese Culture University, Taipei, in 2020, where he is currently pursuing the M.S. degree in mechanical engineering. His research interests include mechatronics, automatic control, and unmanned aerial vehicles.